Korean J. Chem. Eng., 39(3), 596-604 (2022)
DOI: 10.1007/s11814-021-0942-x

pISSN: 0256-1115
eISSN: 1975-7220

A RuO_2IrO_2 electrocatalyst with an optimal composition and novel microstructure for oxygen evolving in the single cell

Feng Ye*, Yanpeng Cao*, Weiwei Han, Yakun Yang*, Yuancheng Feng*, Peng Liu*, Chao Xu*,†, Xiaoze Du*, Woochul Yang**, and Guicheng Liu**,†**

*Key Laboratory of Power Station Energy Transfer Conversion and System of MOE, School of Energy Power and Mechanical Engineering, North China Electric Power University, Beijing 102206, P. R. China
**Department of Physics, Dongguk University, Seoul 04620, Korea
(*Received 8 May 2021 • Revised 16 August 2021 • Accepted 26 August 2021*)

Abstract−A highly active RuO_2IrO_2 electrocatalyst was developed via dip-coating/calcination method for oxygen evolution reaction (OER). The catalyst on Ti substrate with a 7/3 molar ratio between Ru and Ir showed the highest electrocatalytic activity for OER among composite samples in different molar ratios. Moreover, the properties of RuO_2IrO_2 grown on carbon paper were evaluated by proton exchange membrane water electrolysis single cell. Compared with the micron-particle structure of RuO_2IrO_2 catalyst on the Ti substrate, the catalyst grown on the carbon paper showed a novel nano dendrite shape and can be used directly as the gas diffusion electrode. Owing to the large surface area of the catalyst, the nano dendrite-shaped RuO_2IrO_2 catalyst exhibits excellent OER performance in the single cell. Furthermore, a cell voltage of 2.50 V is achieved under 200 mA cm^{-2} at 30 °C by using the optimal composition RuO_2IrO_2 (Ru : Ir=7/3) and the commercial 20% Pt/C as anode and cathode, respectively.

Keywords: Hydrogen Generation, PEM, Oxygen Evolving, Catalytic Activity, RuO_2IrO_2 Catalyst

INTRODUCTION

Nowadays, human beings are suffering from a series of problems, such as energy shortage and environmental pollution. Hydrogen energy, as one of the most promising clean energy sources in the 21st century, has received widespread attention due to its abundant resources and non-pollution [1]. However, it is a key issue to efficiently produce hydrogen energy in international and scientific research [2]. To date, hydrogen has mainly been produced through the centralized transformation of fossil fuels (such as natural gas). For sustainable development, water electrolysis is a better future prospect. Among water electrolysis systems, alkaline electrolysis and proton exchange membrane (PEM) electrolysis systems are considered to have the potential for large-scale hydrogen production using electricity, especially renewable energy [3]. Generally, the PEM electrolysis method separates gas products in pure water, and has the advantages of fast loading response, high yield, and fast startup/shutdown, compared with classical alkaline electrolysis [4]. Nonetheless, the main obstacle of PEM water electrolysis is the large anodic overpotential in the oxygen evolution reaction (OER), which requires a highly active catalyst and hinders its wide applications [5].

In the 1960s, Henry Beer proved that noble metal oxides could be used as electrocatalysts in the form of dimensionally stable anodes (DSA) [6]. Based on the discovery, DSA became a subject of interest for OER because of its low overpotential and inertia characteristics. In general, DSA-type electrodes are composed of two parts: substrate and catalytic coating. Commonly used substrates contain aluminum, oxidation-resisting steel, titanium, and their alloys [7]. Among them, titanium is widely used in three-electrode systems due to its good mechanical stability and relatively low cost. More importantly, an efficient and stable catalytic coating is essential for DSA. At present, conductive metal oxides have been extensively investigated for OER, such as IrO_2, RuO_2, Ta_2O_5, and TiO_2 [8]. For example, Pt-based IrO_2 has shown magnificent performance, but the use of precious metal Pt has hindered its further application [9]. Hence, highly active and low-cost catalysts are still vital for the oxidation of electrolyzed water to evolve O_2.

In recent years, many efforts have been devoted to the synthesis of potential catalysts for water electrolysis [10]. As a typical representative, RuO_2 is regarded as one of the most attractive catalysts for OER due to its high catalytic activity [11]. Moreover, the typical RuO_2-TiO_2 mixtures are favorable for the evolution of Cl_2. Unfortunately, RuO_2 is easily oxidized to unstable RuO_4 at high potential, making the lifespan of RuO_2-TiO_2 DSAs very short during the oxidation reaction process [12]. Regardless of the electrolyte, IrO_2 is a high-performance catalyst for OER comparable to RuO_2, but under acidic conditions, RuO_2 is more active but less stable, while IrO_2 is less active but more stable. Attention is growing about using IrO_x instead of RuO_2 in DSA, owing to the longer lifetime of IrO_2 in acid media [13]. Currently, various IrO_2-based anode catalysts for OER have been promoted, such as ZrO_2IrO_2, TiO_2IrO_2, $PtIrO_2$, and $Ta_2O_5IrO_2$ [14]. Therefore, Ir-containing oxides have gained continuous research concern because of their great potential for OER. For instance, $Ir_xSn_{1-x}O_2$ prepared by Marshall et al. showed out-

†To whom correspondence should be addressed.
E-mail: mechx@ncepu.edu.cn, log67@163.com, liuguicheng@dongguk.edu

standing catalytic performance when used as anode catalyst for OER, exhibiting a current density of 1 A cm^{-2} at 90 °C in the 0.5 M H_2SO_4 and a voltage of 1.65 V [15]. As another example, Tunold's group reported that the cell voltage of $Ir_{0.6}Ru_{0.4}O_2$ was 1.567 V at a higher metal loading of 2.04 mg cm^{-2} at 1 A cm^{-2} and 80 °C [16]. 1.86 V was achieved employing the Pt-IrO_2 at anode under high current density with the total noble metal loading of 0.8 mg cm^2 at 50 °C, reported by Yang [17]. Obviously, high loadings of expensive Pt and Ir oxides limit their practical applications [18]. Moreover, the membrane electrode assembly (MEA) is often prepared by the catalyst coated membrane (CCM) method. For example, Wang et al. constructed a catalyst-coated Nafion membrane by using the spraying method, in which catalyst ink was sprayed onto modified carbon paper and hot-pressing process [19]. The preparation process of CCM is complicated and uncontrollable.

Based on the discussion above, a simple and controllable method was put forward to grow RuO_2IrO_2 directly on the Ti substrate by the dip-coating/calcination method [20]. In the oxide mixture, RuO_2 serves as both dispersant and catalyst, which is significantly different from the traditional method (additional Nafion solution is needed to fix the catalyst on the oxygen electrode). Besides, the composition RuO_2IrO_2 was optimized for OER in a three-electrode system. The performance of the catalyst was evaluated by single-cell tests. The mechanism of the physicochemical properties and the catalytic activity of the coating was analyzed.

EXPERIMENTAL

1. Synthesis of the RuO_2IrO_2/Ti

A Titanium plate (10 mm×10 mm×1 mm) was chosen as the substrate, with an effective area of 1 cm^2. The pretreatment of titanium plate was carried out in the following sequence. First, the Ti substrate was sandblasted, washed by tap water, etched in boiling 3 mol L^{-1} HCl (37%) for 30 min, and cleaned in pure water. Then, 10% oxalic acid was used to etch the cleaned Ti substrate at 90 °C for 1 h. Finally, the etched Ti substrate was rinsed with deionized water.

$RuCl_3$ and $H_2IrCl_6{\cdot}6H_2O$ precursor solutions were prepared, respectively. $RuCl_3$ and $H_2IrCl_6{\cdot}6H_2O$ were dissolved separately in the mixture solution of 2-propanol and ethanol with volume ratio of 1 : 1, i.e., $[RuCl_3]=[H_2IrCl_6]=0.5$ mmol L^{-1}. Then, the precursor solutions were prepared by using the respective solutions above based on the different Ru/Ir molar ratios (i.e., 7/3, 5/5, and 3/7). As a comparison, the $RuCl_3$ precursor solution was obtained by dissolving $RuCl_3$ in the 2-propanol and ethanol solution described above.

On the basis of the pretreatment, the precursor solutions were dripped on the Ti substrate at 20 °C, then dried at 70 °C to evaporate the solvent and finally calcined in air at 450 °C for 10 minutes and cooled naturally to room temperature. The Ti plates repeated the coating, drying, sintering and cooling process as described above. The loading of the metal catalyst coating was controlled by repeating the above process. Finally, the RuO_2IrO_2/Ti electrode was obtained by calcining at 450 °C for 1 hour at a temperature rise rate of 3 °C/min, after which it was naturally cooled to room temperature.

2. Preparation of the RuO_2IrO_2/Carbon Paper Gas Diffusion Layer

RuO_2IrO_2 grown on carbon paper was obtained by the dip-coating/calcination process. The TGP-H-120 carbon paper was initially dipped in the precursor solution (Ru/Ir=7/3) at 20 °C and subsequently dried at 70 °C to vaporize the water and ethanol, and then treated at 450 °C for 10 min. This process was also repeated (about 10-15 times) until the total loading of metal coating reached 0.4 mg cm^{-2}.

3. Fabrication of the Membrane Electrode Assembly (MEA)

To achieve high-performance RuO_2IrO_2 in the PEM water electrolysis, 0.4 mg cm^{-2} metal loading of RuO_2IrO_2 coated on carbon paper was elected as the anode electrode. The commercial 20% Pt/C catalyst was ultrasonically dispersed into Nafion® solution and isopropyl alcohol. Then, the above 20% Pt/C catalyst ink was sprayed on the carbon paper until the metal loading reached 0.4 mg cm^{-2} to obtain the cathode electrode. A MEA of 5 cm^2 was obtained through hot pressing the two electrodes and a Nafion 115 membrane under 75 kg cm^{-2} at 135 °C for 3 min.

4. Electrochemical Measurements

To evaluate the OER activity of RuO_2IrO_2/Ti, cyclic voltammetry (CV) and line polarization measurements were carried out in 0.1 M H_2SO_4 solution. The measurements were performed in the three-electrode system with the RuO_2IrO_2/Ti, saturated calomel electrode (SCE), and Pt plate worked as the working electrode, reference electrode, and counter electrode, respectively. Furthermore, the oxygen evolution properties of the RuO_2IrO_2 electrode were studied in a single cell, in which 0.1 M H_2SO_4 solution was used to evaluate the anodic catalysts. The experiments were carried out on Bio-logic VMP2 at 20 °C.

5. Physical Characterization

Scanning electron microscopy (SEM) was used to observe the microstructure of the as-prepared samples by the ZEISS and LEO-1530 FESEM instruments. Energy-dispersive X-ray spectroscopy (EDS) was employed to verify composition and distribution of the catalyst by Oxford ultim Max65. The phase constitution of the as-

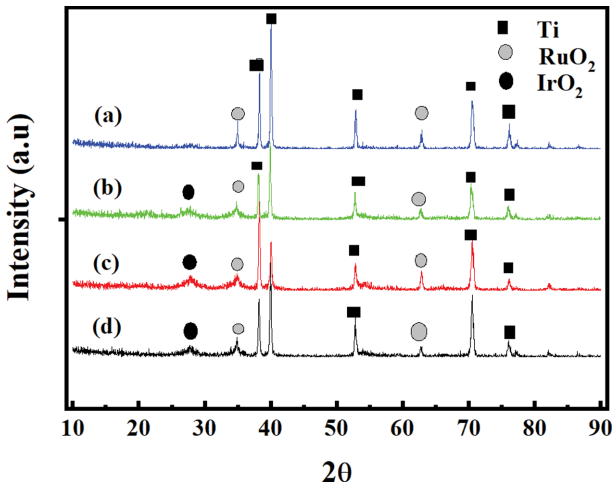

Fig. 1. X-ray diffraction patterns of (a) RuO_2/Ti and RuO_2IrO_2/Ti electrodes with (b) Ru/Ir=3/7, (c) Ru/Ir=5/5, and (d) Ru/Ir=7/3.

synthesized samples was investigated by measuring the X-ray diffraction (XRD) patterns in the MXP21 VAHF system (200 mA Cu KR/35 kV). X-ray photoelectron spectroscopy (XPS) was utilized to analyze the valence states of the major elements with Al Kα radiation by ESCALAB 250Xi.

RESULTS AND DISCUSSION

1. Physical Characterization of the RuO_2/Ti and RuO_2IrO_2/Ti Samples

The XRD patterns of the RuO_2/Ti and RuO_2IrO_2/Ti with vari-

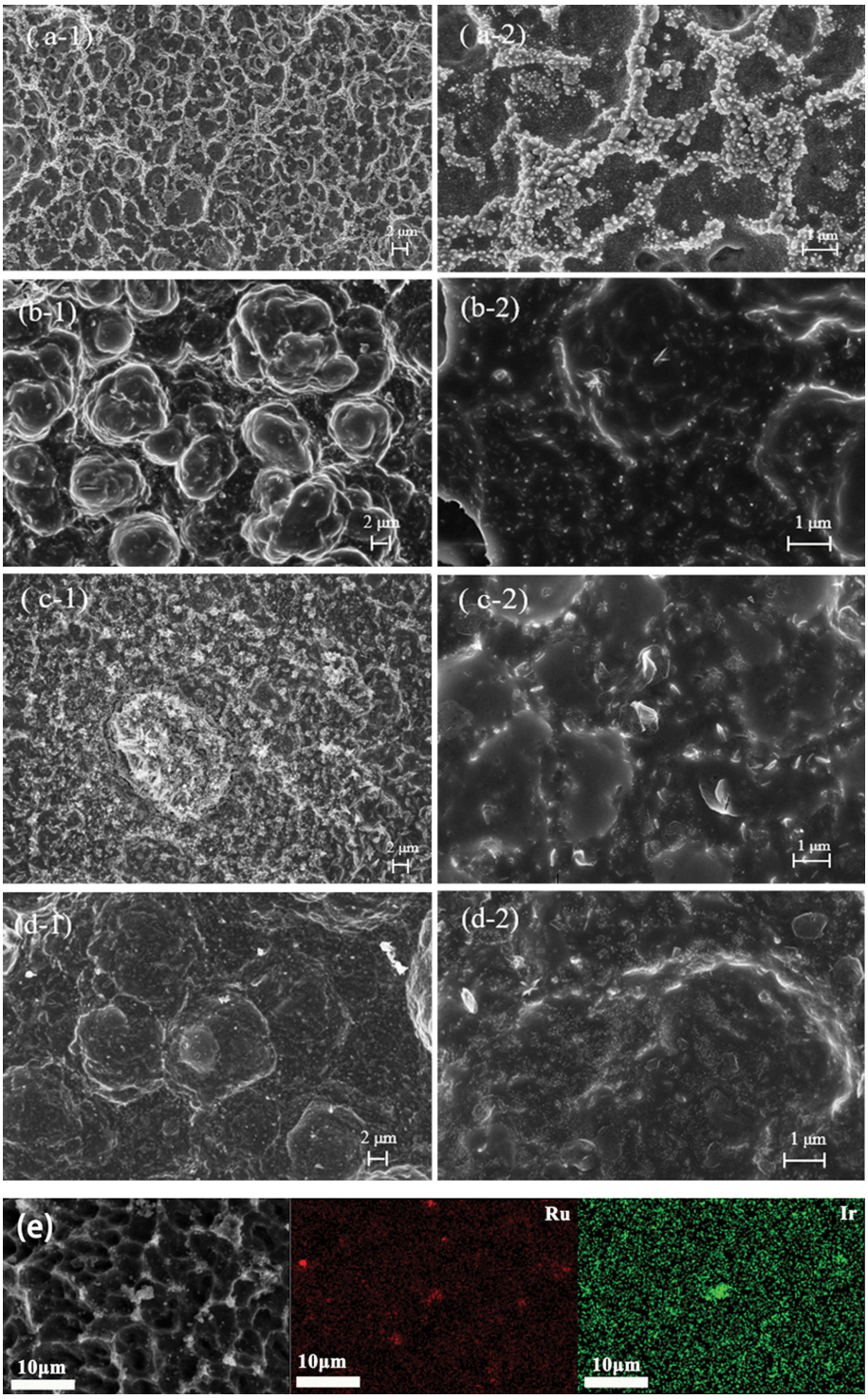

Fig. 2. SEM images of the RuO_2/Ti and RuO_2IrO_2/Ti electrodes in different molar ratio at different magnification (1×5,000; 2×20,000): (a) RuO_2/Ti, (b) RuO_2IrO_2/Ti (Ru/Ir=7/3), (c) RuO_2IrO_2/Ti (Ru/Ir=5/5), and (d) RuO_2IrO_2/Ti (Ru/Ir=3/7), (e) the corresponding element mapping in RuO_2IrO_2/Ti (Ru/Ir=7/3).

ous ratios between Ru and Ir (Ru/Ir=7/3, Ru/Ir=5/5, Ru/Ir=3/7) are displayed in Fig. 1. It proves that the rutile RuO_2 and IrO_2 were synthesized successfully. The intensity from the diffraction peak at 29° was indexed to the rutile-type IrO_2 (JCPDS card No. 880288), and the intensities at 35° and 63° came from the rutile-type RuO_2 (JCPDS card No. 880286). The results show that prepared IrO_2 and RuO_2 possess good crystallinity, which is in accordance with Ref [21]. It was supposed that the $IrCl_6^{2-}$ and $RuCl_3$ were changed into IrO_2 and RuO_2 during the sintering process at 450 °C, respectively [22]. On the other hand, the intense diffraction peaks at 38°, 41°, 53° and 72° were indexed to Ti substrate (JCPDS card No. 882321), suggesting that Ti substrate remained stable. The XRD analysis indicates that no chemical reactions occur between RuO_2, IrO_2, and Ti, demonstrating that RuO_2, IrO_2, and Ti have good chemical compatibility during the preparation of composite oxides.

2. Effect of Composition in the RuO_2IrO_2/Ti Electrodes on the Surface Morphology and the OER Performance

Fig. 2 provides the SEM images of RuO_2/Ti and RuO_2IrO_2/Ti with the Ru/Ir ratios of 7/3, 5/5, and 3/7 synthesized through the dip-coating/calcination method. Obviously, there was no "cracked mud" structure appearing on the Ti surface, which might be related to the sandblast pretreatment of the substrate [23]. In Fig. 2(a), the agglomeration of RuO_2 can be observed. The RuO_2/Ti layer appears to be inhomogeneous. SEM images in Fig. 2(b)-(d) demonstrate RuO_2IrO_2 particles uniformly disperse on the Ti substrate. All surfaces of the RuO_2IrO_2 samples were rough, but the whole feature of these samples was dissimilar to that of RuO_2/Ti, indicating that the film chemical composition could considerably influence the whole morphology. From Fig. 2(b)-(d), it can be seen that the particle size of RuO_2IrO_2 (Ru/Ir=7/3, 5/5, and 3/7) was about 100 nm, 200 nm and 300 nm, respectively. With the increase of Ir content, the RuO_2IrO_2 particles become larger. For the RuO_2IrO_2/Ti with Ru/Ir=7/3, the surface was coated by small star-type catalysts which were interconnected to form a porous structure, suggesting the addition of Ir effectively could improve the coating structure.

In addition, the EDS elemental mapping images reveal the presence of Ru and Ir in RuO_2IrO_2/Ti. Ru oxide and Ir oxide particles were well mixed and uniformly distributed over the entire surface of the titanium plate.

The CV curves of the RuO_2/Ti, RuO_2IrO_2/Ti (Ru/Ir=7/3), RuO_2IrO_2/Ti (Ru/Ir=5/5), and RuO_2IrO_2/Ti (Ru/Ir=3/7) electrode samples were obtained at a scan rate of 100 mV s^{-1} in 0.1 M H_2SO_4 to evaluate the OER of catalysts. From Fig. 3, the sequence of current densities at the same potential in OER was RuO_2IrO_2/Ti (Ru/Ir=7/3)>RuO_2IrO_2/Ti (Ru/Ir=5/5)>RuO_2IrO_2/Ti (Ru/Ir=3/7)>RuO_2/Ti. For example, the current density at 1.6 V ($I_{1.6\,V}$) for the RuO_2IrO_2/Ti (Ru/Ir=7/3), RuO_2IrO_2/Ti (Ru/Ir=5/5), RuO_2IrO_2/Ti (Ru/Ir=3/7) and RuO_2/Ti catalysts was 308.86, 413.24, 501.96, and 253.36 mA cm^{-2}, respectively. Therefore, the RuO_2IrO_2 catalysts were more effective as an OER catalyst compared with the RuO_2. Among these RuO_2IrO_2 catalysts, the oxygen evolution rate increased to the maximum when the atomic Ru/Ir ratio of the catalyst was 7/3. The variation in the voltammogram is bound up with the changes of the catalyst composition and is considered a parameter proportional to the active surface area [24]. The RuO_2IrO_2 (Ru/Ir=7/3) with fine particles may enhance the obvious electrochemical activity [25].

So far, studies have shown that the integrated charge (q*) of the voltammogram in the potential region between HER and OER could characterize the electrochemical activity of oxide-catalyst electrodes [26]. The integrated relationship between q* and the potential (0-1.16 V *vs.* SCE) on the RuO_2/Ti and RuO_2IrO_2/Ti is given in Fig. 4. It can be found that q* of RuO_2IrO_2 is considerably higher than that of RuO_2, illustrating that the active area of the catalyst increases with the addition of IrO_2 into RuO_2. It is possible for the improvement of electrode apparent activity. Moreover, a remarkable increase in q* was found at 70% Ru (atm), followed by a decrease in the integrated charge. When the Ir content in the RuO_2IrO_2/Ti electrodes increased to 30%, q* rose to a maximum of 1,800 mC cm^{-2}, correspondingly. The difference in activity of oxide coatings can be attributed to the following factors: the uniform disper-

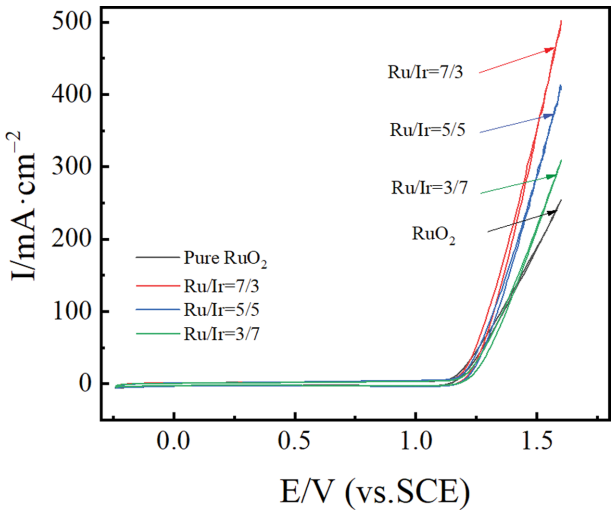

Fig. 3. Cyclic voltammograms at a scan rate of 100 mV s^{-1} for the RuO_2IrO_2/Ti (Ru/Ir=7/3, Ru/Ir=5/5, Ru/Ir=3/7) and RuO_2/Ti electrodes in 0.1 M H_2SO_4 solution.

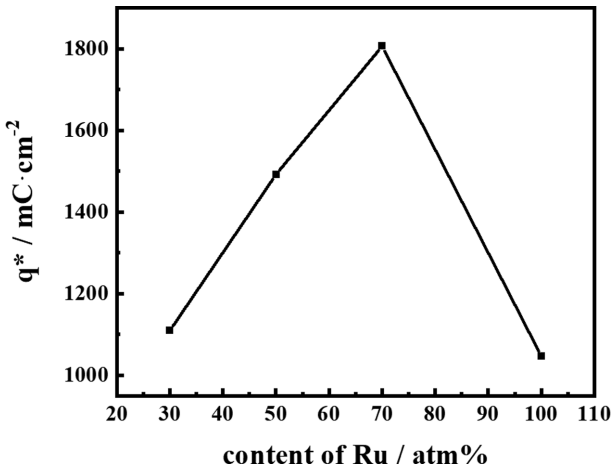

Fig. 4. Integrated voltammetric charges obtained at 100 mV s^{-1} for the RuO_2/Ti and RuO_2IrO_2/Ti electrodes in 0.1 M H_2SO_4 solution on the basis of the Ru content (atm %).

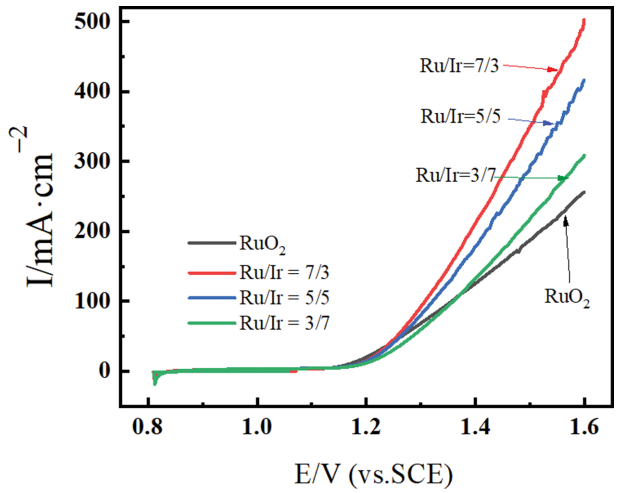

Fig. 5. Polarization curves for the OER of the RuO_2 and RuO_2IrO_2/Ti (Ru/Ir=7/3, Ru/Ir=5/5, Ru/Ir=3/7) electrodes in the range of 0.8-1.6 V *vs.* SCE in 0.1 M H_2SO_4 solution at room temperature.

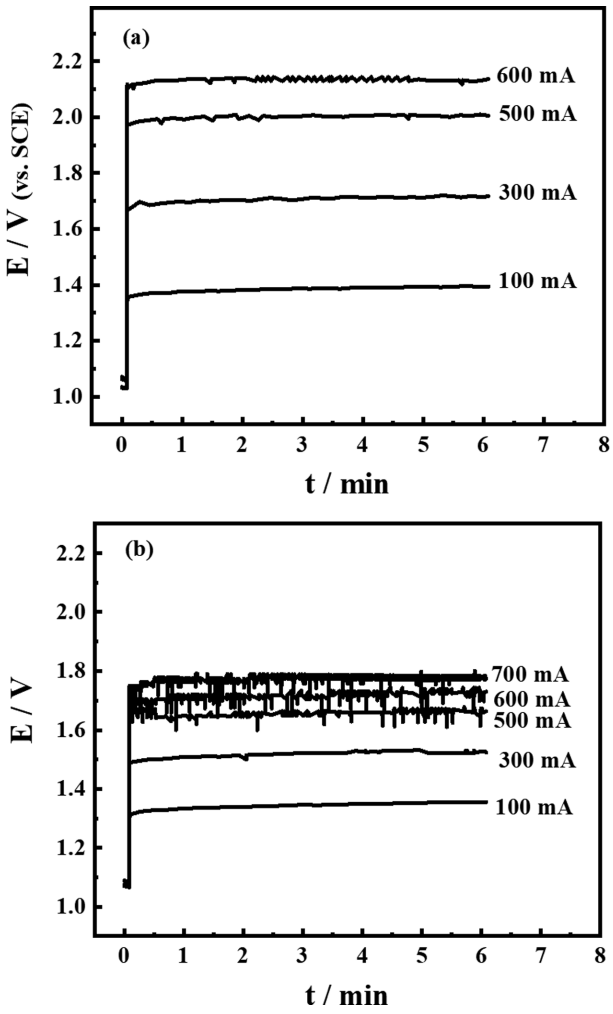

Fig. 6. Chronopotentiometry curves of (a) RuO_2/Ti and (b) RuO_2IrO_2/Ti (Ru/Ir=7/3) electrodes in 0.1 M H_2SO_4 solution at the potential of 1.30 V.

sion particles, large active surface area, and abundant lattice defects. The value of q* stands for the electrocatalytic activity. Thus, the higher the q*, the higher electrocatalytic activity of the electrode. Remarkably, Ir content of 30% in RuO_2IrO_2/Ti electrodes with q* of a maximum 1,800 mC cm^{-2} delivered the highest catalytic activity.

Additionally, the voltammetric charges by CVs curves revealed that there were more active sites on RuO_2IrO_2 catalyst than on RuO_2 catalyst. The change trends in the CVs also demonstrated that the Ru/Ir-based oxides possess a much larger active surface area than the single oxides. Therefore, as a catalyst for the OER, the RuO_2IrO_2 has better performance than the RuO_2. For the RuO_2IrO_2 catalysts, the special active surface area reaches the maximum when the Ru content at 70% (Ru/Ir=7/3).

The electrocatalytic properties of RuO_2/Ti, RuO_2IrO_2/Ti (Ru/Ir=7/3), RuO_2IrO_2/Ti (Ru/Ir=5/5), and RuO_2IrO_2/Ti (Ru/Ir=3/7) for OER were studied by the linear sweep voltammetry test in 0.5 M H_2SO_4 solution, and the results are shown in Fig. 5. It is observed that the current density at 1.6 V ($I_{1.6\,V}$) for the RuO_2/Ti, RuO_2IrO_2/Ti (Ru/Ir=7/3), RuO_2IrO_2/Ti (Ru/Ir=5/5), and RuO_2IrO_2/Ti (Ru/Ir=3/7) catalysts was 255.89, 502.37, 415.82, and 308.86 mA cm^{-2}, respectively. So the peak current density of RuO_2IrO_2/Ti (Ru/Ir=7/3) was 1.96 times higher than that of RuO_2/Ti. This result agrees well with the CV data, demonstrating the RuO_2IrO_2/Ti (Ru/Ir=7/3) with 30% Ir exhibits the best electrocatalytic activity for OER compared to RuO_2IrO_2/Ti (Ru/Ir=5/5, Ru/Ir=3/7) and RuO_2.

From a practical perspective, it is significant to consider the energy efficiency of the electrode surface towards OER, i.e., the larger current value at a given potential. The polarization potentials were estimated with the operating time in 0.1 M H_2SO_4 solution at 20 °C. Different values of the current, from 100 to 700 mA cm^{-2}, were imposed on the electrode (abbreviated as E_{100}, E_{300}, and E_{700}), which represented the potential corresponding to the electrode at the given current density. The oxygen evolution potential of the RuO_2 catalyst and the RuO_2IrO_2 catalysts is given in Table 1. The results show that the OER potential of the RuO_2IrO_2 catalysts

Table 1. Influence of the OER potential on the RuO_2/Ti and RuO_2IrO_2/Ti electrodes under various applied current density

Electrodes	100 mA cm^{-2} (V)	300 mA cm^{-2} (V)	500 mA cm^{-2} (V)	600 mA cm^{-2} (V)	700 mA cm^{-2} (V)
RuO_2	1.41	1.71	2.01	2.14	——
Ru : Ir=7/3	1.35	1.54	1.66	1.72	1.78
Ru : Ir=5/5	1.37	1.55	1.74	1.82	1.90
Ru : Ir=3/7	1.41	1.58	1.71	1.80	1.84

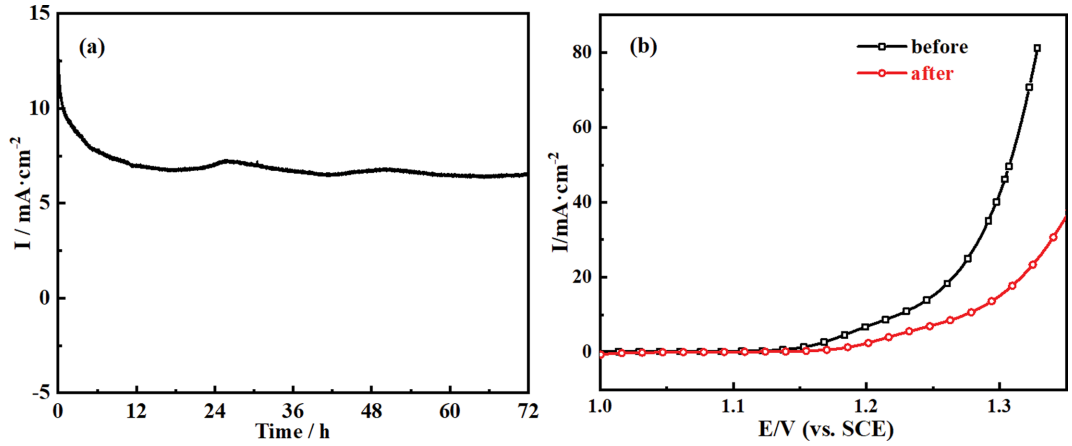

Fig. 7. (a) Chronoamperometric curve of RuO_2IrO_2/Ti (Ru/Ti=7/3) in 0.1 M H_2SO_4 solution at 10 mA cm^{-2}, (b) polarization curves of RuO_2IrO_2/Ti (Ru/Ti=7/3) before and after the chronoamperometric test.

Table 2. Latest catalytic performance table for precious metal catalysts IrO_2 and RuO_2

Catalysts	I/mA cm^{-2}	Overpotential/mV	Electrolyte	Ref.
RuO_2IrO_2/Ti (Ru/Ir=7/3)	10	195	0.1 M H_2SO_4	This work
RuO_2IrO_2/Ti (Ru/Ir=7/3)	10	288	0.1 M H_2SO_4	This work (after stability test)
IrO_2/RGO	5	>420	0.5 M H_2SO_4	[27]
3D ordered macroporous IrO_2	0.5	220	0.5 M H_2SO_4	[28]
3D IrO_2 with dendrite-like structures	10	270	0.5 M H_2SO_4	[29]
Ultrafine IrO_2 nanorods	70	258	0.5 M KOH	[30]
IrO_2-RuO_2@Ru (3 : 1)	100	567	0.5 M H_2SO_4	[31]
Pt-IrO_2 (Pt : Ir=1 : 9)	40.8	514	0.5 M H_2SO_4	[32]
Porous reticular Ru/RuO_2	10	288	1 M KOH	[33]
Mesoporous RuO_2	10	266	0.1 M $HClO_4$	[34]

was smaller than that of the RuO_2 catalyst, which indicates that OER is more likely to occur in the presence of IrO_2-based catalysts. Furthermore, it is found that the OER potential of the RuO_2IrO_2/Ti (Ru/Ir=7/3) electrode was lower than that of the RuO_2IrO_2/Ti (Ru/Ir=5/5, 3/7) with the increase of Ir content at applied current density of 100 and 300 mA cm^{-2}. For example, at an applied current density of 300 mA cm^{-2}, the OER potential of the RuO_2IrO_2/Ti (Ru/Ir=7/3, 5/5, 3/7) electrode was 1.54 V, 1.55 V, and 1.58 V, respectively. It indicates that RuO_2IrO_2/Ti (Ru/Ir=7/3) electrode exhibits higher catalytic activity. As an example, the chronopotentiometry curves of RuO_2/Ti and RuO_2IrO_2/Ti (Ru/Ir=7/3) electrodes in 0.1 M H_2SO_4 are shown in Fig. 6. As for the density of 500 and 600 mA cm^{-2}, the OER potential of the RuO_2IrO_2/Ti (Ru/Ir=7/3) catalysts was 1.65 V and 1.72 V, respectively, which were lower than those of the RuO_2/Ti electrode (2.01 V, 2.14 V). The above results imply that the RuO_2IrO_2 (Ru/Ir=7/3) catalysts show higher electrocatalytic activity for OER. RuO_2IrO_2/Ti (Ru/Ir=7/3) exhibits more effectiveness as the catalytic electrode for OER in water electrolysis in a wide range of current densities. The unique structure and specific interaction between RuO_2 and IrO_2 may be the reason for high electrocatalytic activity. The improvement of electrocatalytic activity of RuO_2 and IrO_2 catalyst may be ascribed to the higher specific surface area, which is well demonstrated by CV results. In addition, to demonstrate the excellent OER catalytic activity of IrO_2/RuO_2 (Ru/Ir=7/3), we compared the OER performance of other recently reported noble metals [27-34], as shown in the Table 2. On one hand, the preparation of bimetallic oxide materials reduces the amount of Ir used and solves the problem of extreme scarcity of Ir. On the other hand, the synergistic effect between the bimetallic oxides improves the OER catalytic activity of the materials.

Stability is a key parameter in determining the industrial exchange of catalysts for applications [35,36]. The stability of the catalyst was evaluated by comparing the change in current density at constant potential and the difference in LSV curves before and after long-term operation. We used the overpotential corresponding to the current density of 10 mA cm^{-2} as the input voltage, and observed the change in current over time. From Fig. 7(a), the current density of RuO_2IrO_2 (Ru/Ir=7/3) decayed from 10 mA cm^{-2} to 6.5 mA cm^{-2} through 72 h of stability testing. The advantage of the interfacial effect of the alloy material combined with the high corrosion resistance of IrO_2 prevented a further reduction in current density [37]. The overpotential of 10 mA cm^{-2} current density was from 195 mV growth to 288 mV (Fig. 7(b)). Even so, it is

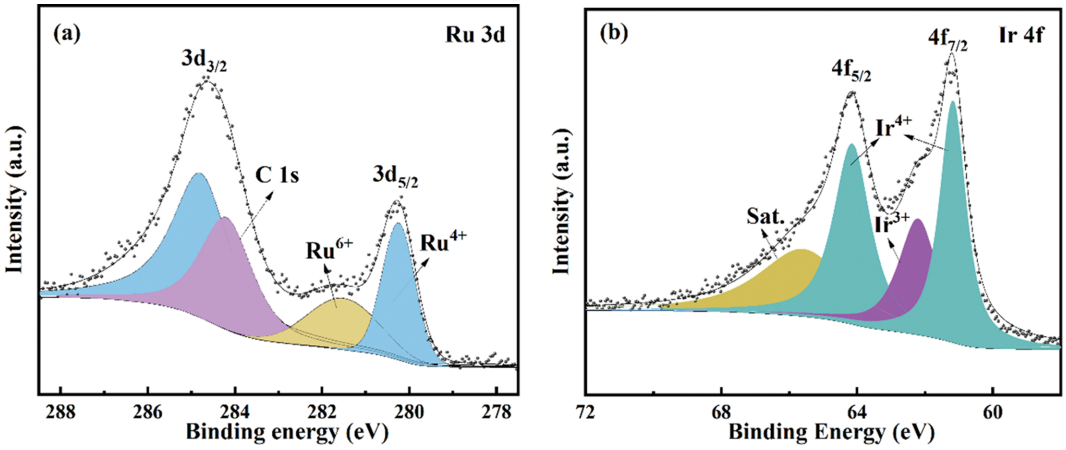

Fig. 8. Typical XPS survey spectra of RuO_2IrO_2/Ti (Ru/Ti=7/3): (a) Ru 3d, (b) Ir 4f.

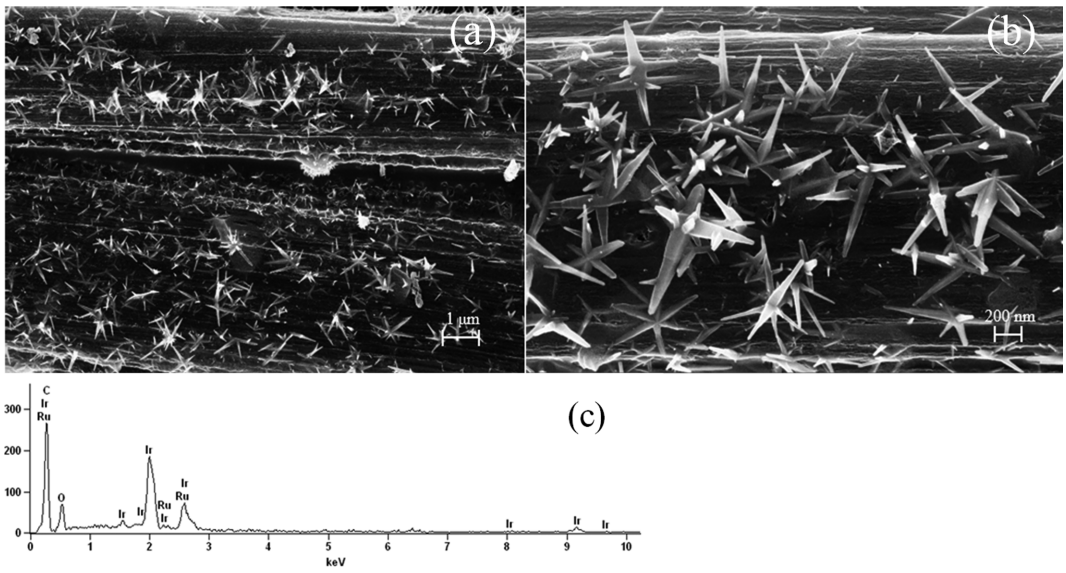

Fig. 9. (a), (b) SEM images of the RuO_2IrO_2/CP (Ru/Ir=7/3) at different magnifications, and (c) EDX analysis of RuO_2IrO_2 nano-dendritic crystal coated on the carbon fiber.

comparable to the catalytic performance of other noble metal catalysts reported in the literature (Table 2).

Fig. 8 shows the XPS spectrum of RuO_2IrO_2/Ti (Ru/Ti=7/3). It demonstrates the presence of Ru and Ir in RuO_2IrO_2/Ti. In the Ru 3d XPS spectra (Fig. 8(a)), the Ru could be found at different chemical valances, with Ru^{4+} $3d_{3/2}$ and Ru^{4+} $3d_{5/2}$ located at 284.2 eV and 280.2 eV, while the location of Ru^{6+} was at 281.5 eV [38,39]. The peak at 284.8 eV corresponding to C1s needs to be split in the spectrum of Ru due to the presence of contaminating carbon [40]. As shown in Fig. 8(b), the peaks centered at 64.35 and 61.38 eV correspond to Ir^{4+} $4f_{5/2}$ and Ir^{4+} $4f_{7/2}$ [41], while the peak at 62.41 eV originated from Ir^{3+} [42]. In addition, one satellite peak at 65.8 eV was also observed. The XPS characterization results show that Ru/Ir does not exist in just one valence state, suggesting that there is a charge transfer between Ru and Ir. It is the change in electronic structure that leads to the enhancement of electron transfer in the catalytic process, which increases the OER catalytic activity of the catalyst.

3. Surface Morphology and Performance of the Optimal Composition RuO_2IrO_2 Supported on the Carbon Paper in a Single Cell

A single cell was fabricated by choosing the optimal RuO_2IrO_2 (Ru/Ir=7/3) as the catalyst for OER. The RuO_2IrO_2 (Ru/Ir=7/3) catalyst was grown directly on the conductive carbon paper by dip-coating/calcination. The morphology and performance of RuO_2IrO_2 (Ru/Ir=7/3) as the anode catalyst on the single cell were explored. Fig. 9 shows the SEM images of the RuO_2IrO_2/carbon paper electrode with 7/3 in Ru/Ir atomic ratio. It can be seen that a uniform distribution of oxidized IrO_2 nano dendritic crystals was formed on the carbon fiber. Of note is that RuO_2IrO_2 directly grows on the carbon paper during the preparation, which is remarkably different from that prepared by the CCM method. The EDX analysis (Fig. 9(c)) confirmed the presence of Ru and Ir in the nano-dendritic crystal with 7/3 in Ru/Ir, which is consistent with the

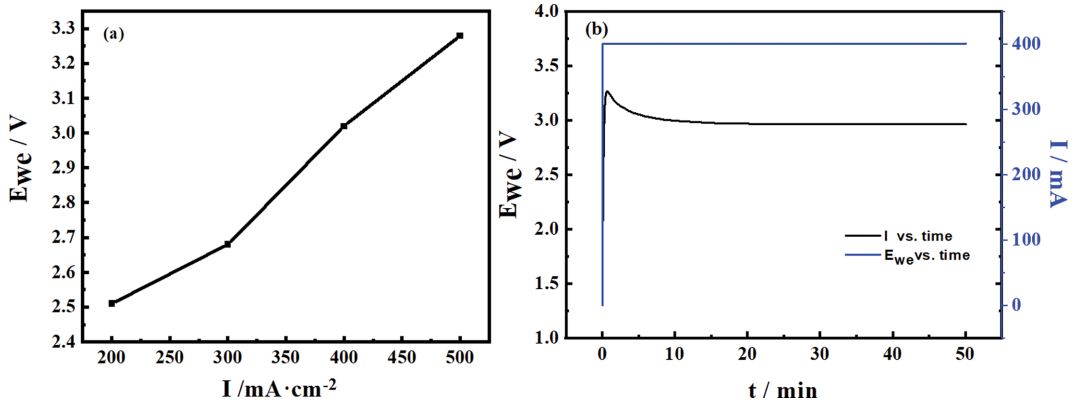

Fig. 10. (a) Performance of the RuO_2IrO_2/carbon paper (Ru/Ir=7/3) based MEA for oxygen electrode in the PEM water electrolysis cell at different applied current density; (b) The performance of RuO_2IrO_2/carbon paper (Ru/Ir=7/3) for oxygen evolution in the PEM water electrolysis cell under the current density of 400 mA cm^{-2} (Note: 0.4 mg cm^{-2} Pt/C as hydrogen electrode; 0.4 mg cm^{-2} RuO_2IrO_2 for oxygen electrode; cell temperature: 30 °C).

metal ratio of the initial precursor salts. Apparently, the method used in this work is beneficial to improve the porosity of the gas diffusion layer and exposure of the catalyst sites. Consequently, a better single cell performance can benefit from the obvious improvement of gas-liquid two-phase mass transfer properties.

The RuO_2IrO_2 coated on conductive carbon paper with 0.4 mg cm^{-2} metal loading was made as to the basis for MEA preparation. The performance of the electrolytic cell was evaluated in a pure water electrolyte at 30 °C. The variations of the single cell voltage with time under different current densities are provided in Fig. 10. It is significantly obvious that the low current density of 200 mA cm^{-2} corresponds to a cell voltage of 2.5 V for the water electrolysis cell (Fig. 10(a)). Meanwhile, there is a positive correlation between cell voltage and current density. Fig. 10(b) shows the performance of the catalyst for OER in the PEM water electrolysis cell at a higher current density of 400 mA cm^{-2}. The corresponding cell voltage of a single cell reached up to 2.9 V. In principle, a high current density corresponds to a large overpotential, which leads to a reduction in the performance of the single cell, especially for the oxygen electrode. Furthermore, the stability of the water electrolysis cell remained good with the increase of operation time. The results indicate that RuO_2IrO_2 with nano dendritic crystal structure on the anode side is directly grown on the carbon paper with the unified whole structure.

CONCLUSIONS

In summary, we proposed a feasible preparation strategy to grow RuO_2IrO_2 directly on the Ti substrate by using the dip-coating/calcination method without the addition of the classical sprayed ink. The effects of the composition of the catalytic electrode on the morphology and electrochemical performance of RuO_2IrO_2 were investigated systematically. The obtained RuO_2IrO_2 showed uniform nano dendritic crystal structure. The combination of IrO_2 and RuO_2 significantly improved OER activity. Meanwhile, results showed that the optimal molar ratio between Ru and Ir in the RuO_2IrO_2 electrocatalyst was 7/3. As expected, a cell voltage as low as 2.50 V was barely required current density of 200 mA cm^{-2} when the RuO_2IrO_2 (Ru/Ir=7/3) with 0.4 mg cm^{-2} metal loading and 20% Pt/C as the anode and cathode catalyst, respectively. Overall, such a great comprehensive performance of the electrode has a great potential prospect in the PEM water electrolysis application field.

ACKNOWLEDGEMENTS

This work was supported by National Natural Science Foundation of China (No. 21476246, and No. 51821004), the Brain Pool program funded by the Ministry of Science and ICT through the National Research Foundation of Korea (No. 2019H1D3A2A02100593), the National Research Foundation of Korea (NRF) grant funded by the Korea government (MSIT) (No. 2019R1C1C1006310, and No. 2021K2A9A2A06044652), and the Fundamental Research Funds for the Central Universities, China (No. 2018ZD04).

REFERENCES

1. H. Kim, H. Park, H. Bang and S. K. Kim, *Korean J. Chem. Eng.*, **37**, 1275 (2020).
2. M. Wang, M. Chen, Z. Yang, G. Liu, J. K. Lee, W. Yang and X. Wang, *Energy Convers. Manage.*, **191**, 132 (2019).
3. H. Kim, J. Kim, G. H. Han, H. W. Jang, S. Y. Kim and S. H. Ahn, *Korean J. Chem. Eng.*, **37**, 1340 (2020).
4. E. Brightman, J. Dodwell, N. V. Dijk and G. Hinds, *Electrochem. Commun.*, **52**, 1 (2015).
5. D. Rosestolato, J. Fregoni, S. Ferro and A. de Battisti, *Electrochim. Acta*, **139**, 180 (2014).
6. H. B. Beer, *British Patent* 1,147,442 (1969).
7. G. P. Vercesi, J. Rolewicz and C. Comninellis, *Thermochim. Acta*, **176**, 31 (1991).
8. R. Z. Aleksandar, V. Edgar, M. Justus and S. Wolfgang, *J. Electroanal. Chem.*, **828**, 63 (2018).
9. F. Ye, J. Li, X. Wang, T. Wang, S. Li, H. Wei, Q. Li and E Christensen, *Int. J. Hydrogen Energy*, **35**, 8049 (2010).
10. B. M. Hunter, H. B. Gray and A. M. Muller, *Chem. Rev.*, **116**, 14120 (2016).

11. Y. Lee, J. Suntivich, K. J. May, E. E. Perry and Y. Shaohorn, *J. Phys. Chem. Lett.*, **3**, 399 (2012).
12. G. Lodi, E. Sivieri, A. Battisti and S. Trasatti, *J. Appl. Electrochem.*, **8**, 135 (1978).
13. W. Xu, G. M. Haarberg, F. Seland, S. Sunde, A. P. Ratvik, S. Holmin, J. Gustavsson, Å. Afvander, E. Zimmerman and T. Åkre, *Corr. Sci.*, **150**, 76 (2019).
14. D. Chun, C. R. Lim, H. S. Lee, W. S. Yoon, T. K. Lee and D. K. Kim, *J. Water Process Eng.*, **26**, 1 (2018).
15. A. Marshall, B. Børresen, G. Hagen, M. Tsypkin and R. Tunold, *Electrochim. Acta*, **51**, 3161 (2006).
16. A. T. Marshall, S. Sunde, M. Tsypkin and R. Tunold, *Int. J. Hydrogen Energy*, **32**, 2320 (2007).
17. F. Ye, W. Hu, H. Liu, J. Liu, J. Li, X. Wang and J. Yang, *Asia-Pac J. Chem. Eng.*, **8**, 271 (2013).
18. J. Lee, B. Jeong and J. D. Ocon, *Curr. Appl. Phys.*, **13**, 309 (2013).
19. G. Liu, Z. Yang, M. Halim, X. Li, M. Wang, J. Y. Kim, Q. Mei, X. Wang and J. K. Lee, *Energy Convers. Manage.*, **138**, 54 (2017).
20. N. Negishi, S. Matsuzawa, K. Takeuchi and P. Pichat, *Chem. Mater.*, **19**(15), 3808 (2007).
21. W. F. McClune, *Powder diffraction file alphabetical index inorganic phase*, JCPDS, Swarthmore, PA (1980).
22. H. Mazhari, K. Jafarzadeh and S. M. Mirali, *J. Electroanal. Chem.*, **777**, 67 (2016).
23. A. Olivera-Sousa, M. A. S. Silva, S. A. S. Machado, L. A. Avaca and P. Lima-Neto, *Electrochim. Acta*, **45**(27), 4467 (2000).
24. C. Angelineta, S. Trasatti, L. D. Atanasoska and R. T. Atanasoski, *J. Electroanal. Chem.*, **214**(1-2), 535 (1986).
25. A. J. Terezo and E. C. Pereira, *Electrochim. Acta*, **44**(25), 4507 (1999).
26. L. A. Da Silva, V. A. Alves, S. Trasatti and J. F. C. Boodts, *J. Electroanal. Chem.*, **427**(1-2), 97 (1997).
27. F. D. Kong, Z. Sheng, G. P. Yin, L. Jing and Z. Q. Xu, *Int. J. Hydrogen Energy*, **38**, 9217 (2013).
28. F. Liu, X. Sun, X. Chen, C. Li and J. Yu, *Polymers*, **11**(4), 629 (2019).
29. C. Cai, S. Han and Y. Tang, *Sustain. Energy Fuels*, **4**, 2462 (2020).
30. J. Ahmed and Y. Mao, *Electrochim. Acta*, **212**, 686 (2016).
31. G. Li, S. Li, J. Ge, C. Liu and X. Wei, *J. Mater. Chem. A*, **5**, 17221 (2017).
32. Z. M. Wang, P. Liu, Y. P. Cao, F. Ye and X. Z. Du, *Int. J. Energy Res.*, **45**, 5841 (2020).
33. J. Hu, Y. Fu, P. Yang, L. Guo, S. Ye, X. Ren, C. He, Q. Zhang and J. Liu, *Mater. Charact.*, **177**, 111201 (2021).
34. S. W. Lee, C. Baik and C. Pak, *Catal. Today*, **358**, 203 (2019).
35. Y. Pi, Q. Shao, P. Wang, F. Lv, S. Gu, J. Guo and X. Huang, *Angew. Chem.*, **56**, 4502 (2017).
36. A. Tahira, Z. H. Ibupoto, M. Vagin, U. Aftab, M. I. Abro, M. Willander and O. Nur, *Catal. Sci. Technol.*, **9**, 2879 (2019).
37. C. Wang, L. Jin, H. Shang, H. Xu and Y. Du, *Chin. Chem. Lett.*, **32**, 2108 (2020).
38. Y. Fan, X. Zhang, Y. Zhang, X. Xie and S. Lu, *J. Colloid Interface Sci.*, **604**, 508 (2021).
39. J. Shan, C. Guo, Y. Zhu, S. Chen, L. Song, M. Jaroniec, Y. Zheng and S. Z. Qiao, *Chem*, **5**, 445 (2019).
40. Y. Tian, S. Wang, E. Velasco, Y. Yang, L. Ca O, L. Zhang, X. Li, Y. Lin, Q. Zhang and L. Chen, *Science*, **23**, 100756 (2020).
41. M. K. Kundu, R. Mishra, T. Bhowmik, S. Kanrar and S. Barman, *Int. J. Hydrogen Energy*, **45**, 6036 (2020).
42. Y. Zhang, Q. Ma, K. Feng, J. Guo and T. Lin, *Ceram. Int.*, **46**, 17640 (2020).